

Cross section and vector analyzing power iT_{11} of the processes ${}^3\text{He}(\vec{d}, d){}^3\text{He}$ (\vec{d}, p) ${}^4\text{He}$ between 15 and 40 MeV

R. Roy*

*Lawrence Berkeley Laboratory, University of California, Berkeley, California 94720
and Laboratoire de Physique Nucléaire, Université Laval, Québec, Canada, G1K 7P4*

F. Seiler,[†] H. E. Conzett, and F. N. Rad[‡]

Lawrence Berkeley Laboratory, University of California, Berkeley, California 94720

(Received 6 April 1981)

Differential cross sections $\sigma_0(\theta)$ and angular distributions of the vector analyzing power $iT_{11}(\theta)$ have been measured for the processes ${}^3\text{He}(\vec{d}, d){}^3\text{He}$ and ${}^3\text{He}(\vec{d}, p){}^4\text{He}$ from 15 to 40 MeV in intervals of 5 MeV. Data were obtained typically at 25 to 35 angles. In both reactions the angular distributions of the observables, expanded in terms of Legendre polynomials, clearly show structure near 20 and 35 MeV. In addition, an optical model fit to the elastic scattering data was used in an attempt at a distorted-wave Born approximation analysis of the reaction data.

[NUCLEAR REACTIONS ${}^3\text{He}(\vec{d}, d){}^3\text{He}$, ${}^3\text{He}(\vec{d}, p){}^4\text{He}$, $E_d = 14.6$ to 39.9 MeV, measured vector analyzing power $iT_{11}(E_d, \theta)$ and cross section $\sigma_0(E_d, \theta)$. Optical model and DWBA analysis.]

I. INTRODUCTION

The mass-five system has been the object of numerous experimental and theoretical studies in the past several years.¹⁻³ The availability of polarized deuteron beams and polarized ${}^3\text{He}$ targets has allowed a detailed experimental study of the systems $\vec{d} + {}^3\text{H}$ (Refs. 4 and 5) and $\vec{d} + {}^3\text{He}$ (Refs. 6 and 7) as well as $d + {}^3\text{He}$ (Refs. 8-10) and $\vec{d} + {}^3\text{He}$ (Ref. 11). Measurements of the polarization of the outgoing nucleon¹²⁻¹⁵ and polarization transfer experiments ${}^3\text{H}(\vec{d}, \vec{n}){}^4\text{He}$ and ${}^3\text{He}(\vec{d}, \vec{p}){}^4\text{He}$ have also been carried out at several energies.^{5,16-19} Recently, sources of polarized tritons and ${}^3\text{He}$ particles have become operational, considerably broadening the range of investigations.²⁰⁻²² With measurements of all these observables available, complete experiments are a distinct possibility.^{23,24} In addition, precise phase-shift analyses of nucleon- ${}^4\text{He}$ elastic scattering^{25,26} up to 55 MeV and a variety of other nuclear reactions have provided detailed information on the intermediate system over a wide range of excitation energies.³ On the theoretical side microscopic calculations, using a cluster approach, have been very successful in

providing new insights into the structure of the five-nucleon system and the processes in which it is formed.²⁷⁻³¹

The ${}^3\text{He}(d, p){}^4\text{He}$ reaction is a particularly suitable process for both theoretical and experimental investigations. Its spin structure is already quite complex, but polarized beams or targets can be prepared for all reactants with spin, making a large number of observables available for a detailed comparison of theory and experiment. The present work extends the range of vector polarization studies of the processes ${}^3\text{He}(\vec{d}, d){}^3\text{He}$ and ${}^3\text{He}(\vec{d}, p){}^4\text{He}$ from 15 to 40 MeV in 5 MeV intervals. Complete differential cross sections $\sigma_0(\theta)$ and angular distributions of the vector analyzing power $iT_{11}(\theta)$ have been measured at all energies. Cross sections and angular distributions of polarization for both processes were analyzed in terms of Legendre polynomials. The resulting coefficients were investigated for energy-dependent features such as those predicted by some analyses and models.^{27,30-32} In addition, the elastic scattering data were fitted with an optical model code, while the reaction data were parametrized by distorted-wave Born approximation (DWBA) calculations.

II. EXPERIMENTAL ARRANGEMENT

A purely vector polarized beam of the Berkeley 88-inch cyclotron impinged on a ^3He gas target in a 91-cm scattering chamber. The beam polarization was monitored in a $^4\text{He}(d,d)^4\text{He}$ polarimeter located further downstream. Typically, about 80% of the maximum possible value ($P_y = \frac{2}{3}$) was found, using a calibration published earlier.³³ During a run the polarization usually remained constant to within 0.01.

The detection system consisted of three detector arrangements mounted 10° apart on each side of the beam. At the most forward angle an $E\text{-}\Delta E$ telescope allowed the simultaneous identification of ^3He and ^4He recoils from the $^3\text{He}(d,d)^3\text{He}$ and $^3\text{He}(d,p)^4\text{He}$ processes, respectively. The second system consisted of two detectors to measure the deuteron and proton spectra separately, using appropriate aluminum absorbers to separate deuterons from ^3He particles. The third system was a single detector with an absorber thick enough to stop all reaction partners except protons. Two fixed detectors, set at $\theta = 22^\circ$ and placed at $\pm 7^\circ$ with respect to the normal to the scattering plane, provided a relative normalization between individual runs. At each energy a run with an unpolarized beam provided an absolute measurement of the cross sections and thus allowed a calibration of the monitors.

The peaks in the spectra at the lower energies were usually very well separated, allowing straightforward summation over the peaks. Background subtraction was needed with increasing energy, predominantly at forward angles. For those spectra, a smoothly varying function was used to represent the background, which was generally small, relatively to the peaks of interest in that angular region of large cross sections. Dead time corrections were applied, amounting to several percent for some of the forward angle data. The systematic errors of the cross sections for both processes are estimated to be less than 10%.

III. RESULTS

The present data for elastic scattering are in satisfactory agreement with measurements of cross sections and vector analyzing power^{34,35} at lower energies (Figs. 1 and 2). At comparable energies the cross sections agree well with available data³⁵⁻³⁷ except at 39.2 MeV ,³⁶ where there is a

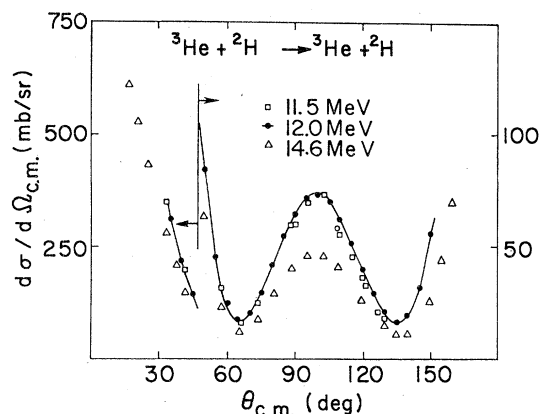


FIG. 1. Comparison of the present cross-section data for the $^3\text{He}(d,d)^3\text{He}$ reaction at 14.6 MeV laboratory energy (Δ) with the data of König *et al.* at 11.5 MeV (\square , Ref. 34) and King and Smythe at 12.0 MeV ($\text{---}\bullet\text{---}$, Ref. 35).

discrepancy in the dip near c.m. angles of $100^\circ - 110^\circ$.

The cross sections of the $^3\text{He}(d,p)^4\text{He}$ reaction presented here are systematically lower than those of King and Smythe³⁵ and those derived from measurements of the inverse reaction at 35 MeV.³⁸⁻⁴⁰ However, there is good agreement with other cross-section values at 25 MeV,³⁷ and both observables join smoothly to values at lower energies (Figs. 3 and 4) measured by the Zürich group.⁴¹

The present data, summarized in Figs. 5 and 6, show few and only gradual changes in the angular

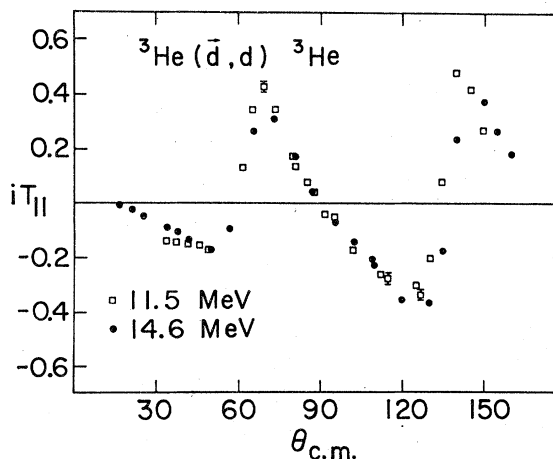


FIG. 2. Comparison of the present vector analyzing power data for the $^3\text{He}(\bar{d},d)^3\text{He}$ reaction at 14.6 MeV (\bullet) with the data of König *et al.* (\square , Ref. 34) at 11.5 MeV.

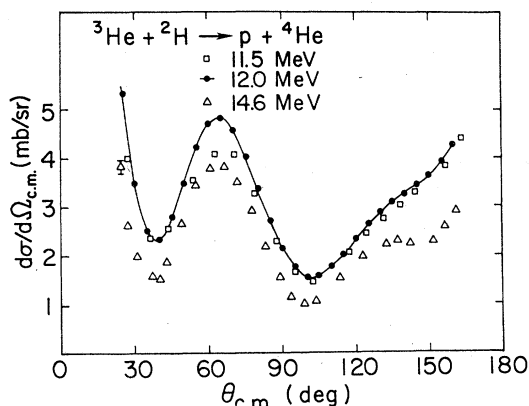


FIG. 3. Comparison of the present cross section data for the ${}^3\text{He}(d,p){}^4\text{He}$ reaction at 14.6 MeV laboratory energy (Δ) with the data of Gruebler *et al.* at 11.5 MeV (\square , Ref. 41) and King and Smythe at 12.0 MeV (\bullet , Ref. 35).

distributions of both observables. The vector analyzing power reaches relatively large fractions of the maximum possible values ($iT_{11} = \pm \frac{1}{2}\sqrt{3}$), mostly at rear angles for elastic scattering but at forward angles for the proton reaction. In the latter the angular distribution of iT_{11} , which is essentially antisymmetric with regard to 90° at 11.5 MeV and below (Refs. 7 and 41, and Fig. 4), changes to a more symmetric appearance between 20 and 30 MeV. The elastic scattering data, on the other hand, show little change over the entire region.

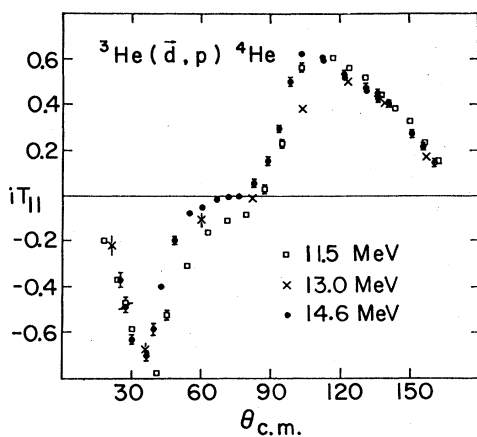


FIG. 4. Comparison of the vector analyzing power data at 14.6 MeV laboratory energy (\bullet , present work) with the data of Gruebler *et al.* (Ref. 41) at 11.5 MeV (\square) and Klinger *et al.* (Ref. 42) at 13.0 MeV (\times).

IV. ANALYSIS

A. Discussion of the Legendre polynomial fits

Both the cross sections $\sigma_0(\theta)$ and the quantities $C_{11}(\theta) = -2iT_{11}(\theta)\sigma_0(\theta)$, derived from the vector analyzing power, were parametrized by expansions in terms of appropriate Legendre polynomials. The normalized expansion coefficients $d_{00}(L)$ and $d_{11}(L)$ are then given by³⁰

$$\frac{4\pi}{\sigma_{\text{tot}}}\sigma_0(\theta) = \sum_L d_{00}(L)P_{L,0}(\cos\theta),$$

$$\frac{4\pi}{\sigma_{\text{tot}}}\sigma_0(\theta)[-2iT_{11}(\theta)] = \sum_L d_{11}(L)P_{L,1}(\cos\theta).$$

The maximum degree L_m of the polynomials used was determined in the usual manner, except in cases where a generally nonzero coefficient crosses zero as a function of energy. In these circumstances that particular coefficient was also allowed to vary freely. The values of maximum degree L_m , determined in this manner, varied between 8 and 12. With 25 to 35 data points per angular distribution, the resulting degrees of freedom of the fits were sufficiently large for a reliable determination of the coefficients. In Figs. 7 and 8 they are given for ${}^3\text{He}(d,d){}^3\text{He}$ elastic scattering and in Figs. 9 and 10 for the ${}^3\text{He}(d,p){}^4\text{He}$ reaction. The resulting fits are shown as the solid lines in Figs. 5 and 6, while the total cross sections derived from the analysis are given in Fig. 11 and Table I. The values of the coefficients for the ${}^3\text{He}(d,p){}^4\text{He}$ reaction below 11.5 MeV were taken from the work of the Zürich group.⁷ Mostly, they establish a trend leading directly to the values presented here.

The cross section $\sigma_0(\theta)$ for elastic scattering of the deuterons shows a strong energy-dependent structure of the coefficients $d_{00}(L)$ near 35 MeV and a weaker one near 20 MeV (Fig. 7). While almost all coefficients are strongly affected at the higher energy, the structure near 20 MeV shows best in the coefficients of higher degree L . A similar situation obtains for the cross section of the ${}^3\text{He}(d,p){}^4\text{He}$ reaction (Fig. 9). The structure at higher energies, however, is not nearly as dominant, while the one at the lower energy affects again all coefficients.

The expansion coefficients $d_{11}(L)$ show quite generally less structure. In elastic scattering (Fig. 8) they are small and do not vary strongly with energy, although they show perturbations near both 20 and 35 MeV. In the ${}^3\text{He}(\bar{d},p){}^4\text{He}$ reaction, almost no corresponding structure can be discerned

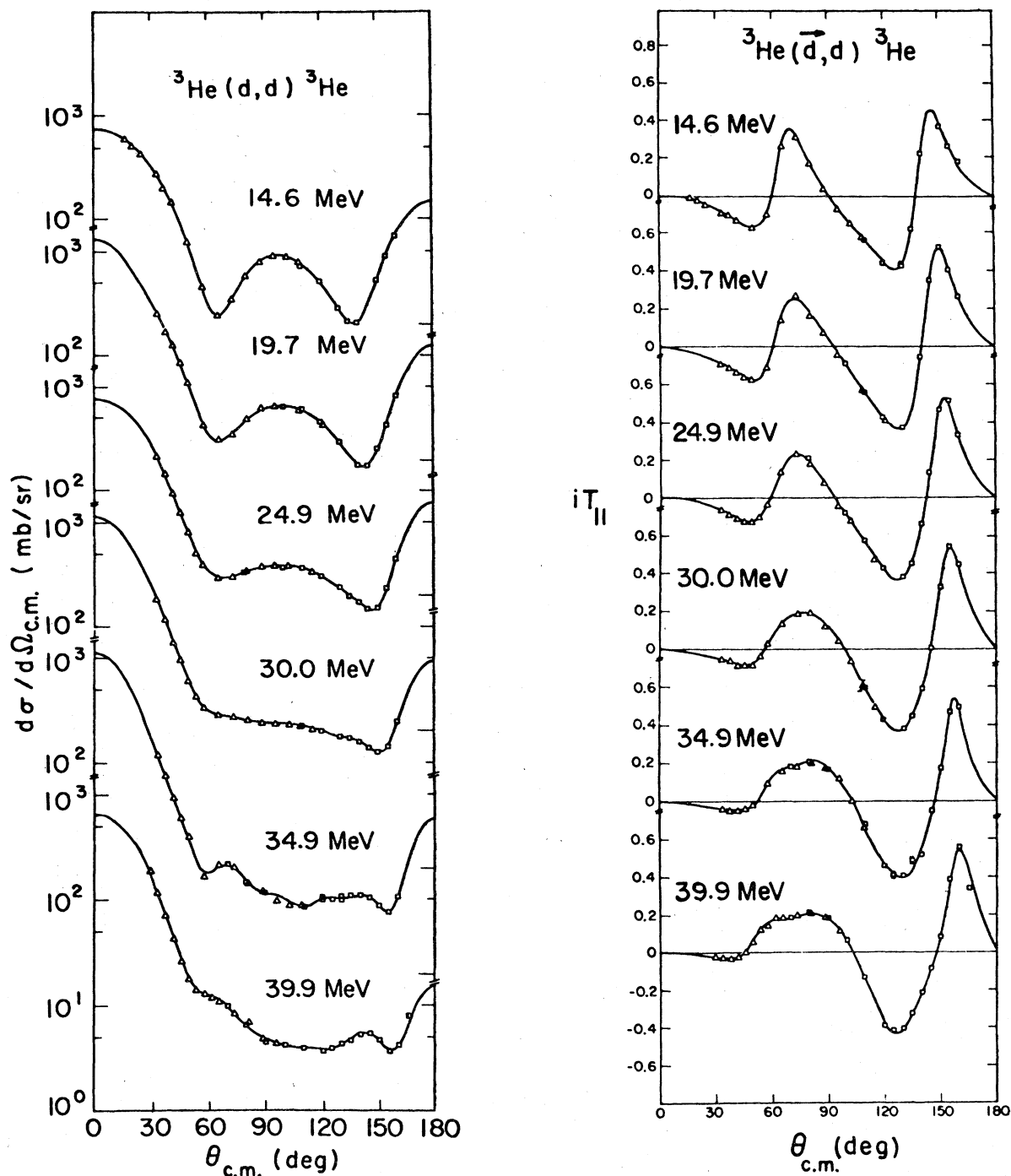


FIG. 5. Angular distributions of the cross section and the vector analyzing power iT_{11} for the ${}^3\text{He}(d,d){}^3\text{He}$ reaction between 14.6 and 40 MeV laboratory energy. The squares represent the angles measured using the recoil ${}^3\text{He}$ particles. The symbol is larger than the statistical error when no error bars are shown. The solid lines are the best Legendre polynomial fits.

at 35 MeV, while the one at 20 MeV is very weak (Fig. 10). In this process, however, the main energy dependent features are shown by the coefficients $d_{11}(1)$ and $d_{11}(2)$. At low energies the $L=2$ term

is large and dominates all others. As the energy increases toward 20 MeV, it goes to small values, while the initially unimportant $L=1$ coefficient becomes large enough to determine the gross struc-

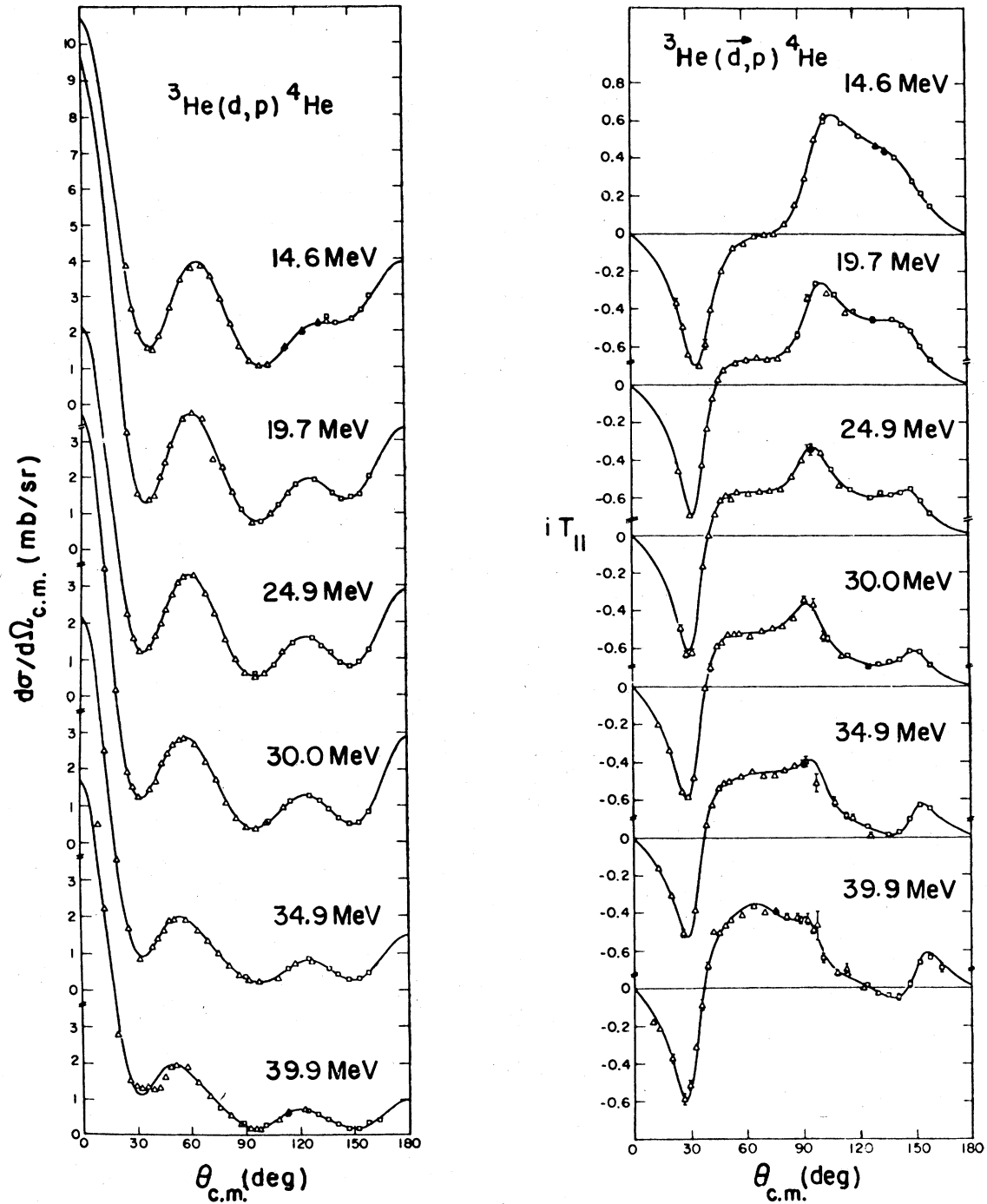


FIG. 6. Differential cross section and vector analyzing power for the ${}^3\text{He}(d,p){}^4\text{He}$ reaction between 14.6 and 40 MeV. The recoil alpha particles were detected at angles represented by squares. The symbol is larger than the statistical error when no error bars are shown. The solid lines are the best Legendre polynomial fits.

ture of the angular distribution.

This change can be interpreted in terms of intermediate states in the ${}^5\text{Li}$ system.^{3,30,31} An expansion coefficient $d_{kq}(L)$ is a linear combination of a

set of interference terms $R_1 R_2^*$ of reaction amplitudes $R_i \equiv \langle l'_i, s'_i, J_i^\pi | R | l_i, s_i, J_i^\pi \rangle$. A restriction required by parity conservation for all first order and some second order polarization observables³⁰ is

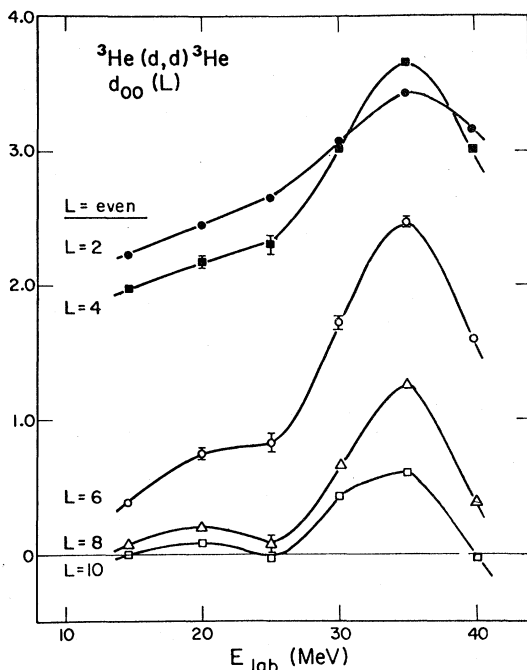
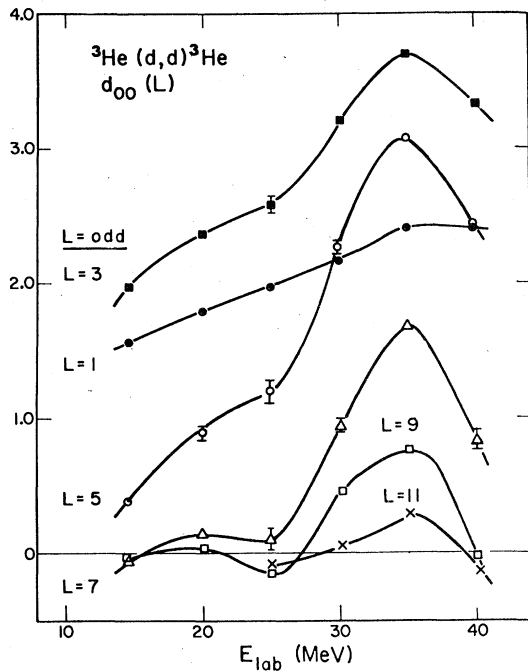


FIG. 7. The parameters $d_{00}(L)$ of the Legendre polynomial expansion corresponding to the fits shown in Fig. 5 for ${}^3\text{He}(d,d){}^3\text{He}$ scattering. When no error bars are shown, the uncertainties of the fits are larger than the symbol. The solid lines are drawn by hand to guide the eye.

that the interference term must satisfy the condition $l_1 + l_2 + L = \text{even}$. Therefore, the even L terms involve combinations of reaction matrix elements with equal parity, while opposite parities

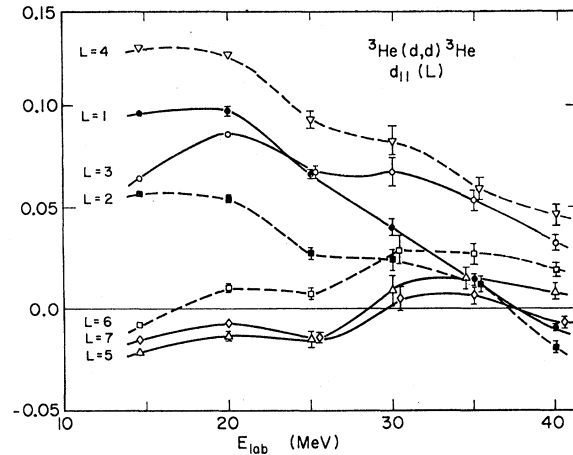


FIG. 8. The parameters $d_{11}(L)$ of the Legendre polynomial expansion corresponding to the fits shown in Fig. 5 for the ${}^3\text{He}(\vec{d},d){}^3\text{He}$ data. Uncertainties larger than the size of a symbol are shown. The solid lines are drawn by hand to guide the eye.

lead to contributions to the odd L coefficients. The predominance of the coefficients $d_{11}(2)$ thus supports the result of calculations by Heiss and Hackenbroich,²⁷ which leads to strong interference

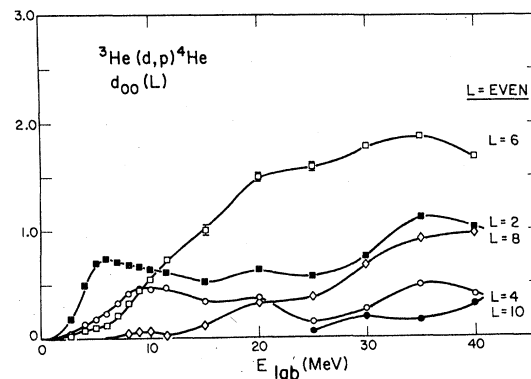
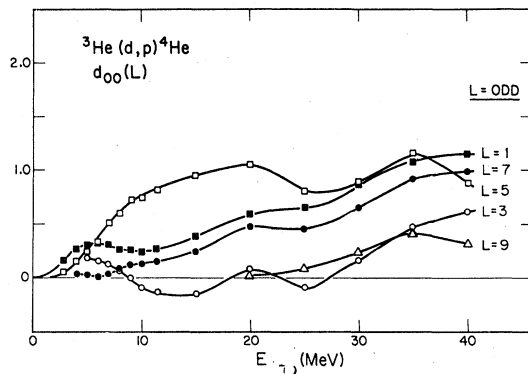


FIG. 9. The parameters $d_{00}(L)$ for the ${}^3\text{He}(\vec{d},p){}^4\text{He}$ data of Fig. 6. The values of the coefficients below 12 MeV were taken from Ref. 41.

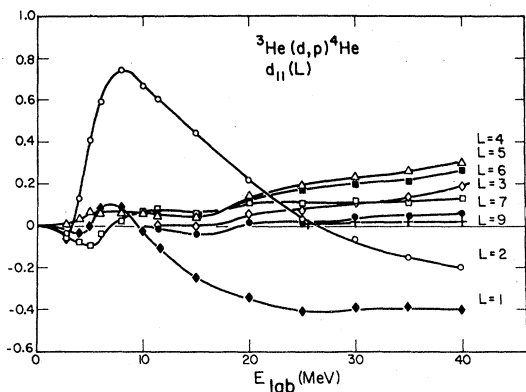


FIG. 10. The parameters $d_{11}(L)$ for the ${}^3\text{He}(\vec{d},p){}^4\text{He}$ data of Fig. 6. The values of the coefficients below 12 MeV were taken from Ref. 41.

terms between members of a quartet of d -wave resonances. Further experimental evidence is supplied by two recent analyses of the reaction.^{30,31} Correspondingly, the rise in importance of the $L=1$ coefficient with increasing energy is due to terms involving matrix elements of opposite parity, such as the d -wave amplitudes and large f -wave $\frac{7}{2}$ state proposed at deuteron energies above 11.5 MeV. A further preliminary analysis along such lines³⁰ must await the measurement of the analyzing power for deuteron tensor polarization.

B. Optical model fit of ${}^3\text{He}(\vec{d},d){}^3\text{He}$

It has been pointed out⁴³ that the similarity of deuteron scattering from ${}^3\text{He}$ and ${}^4\text{He}$ above $E_d \sim 8$

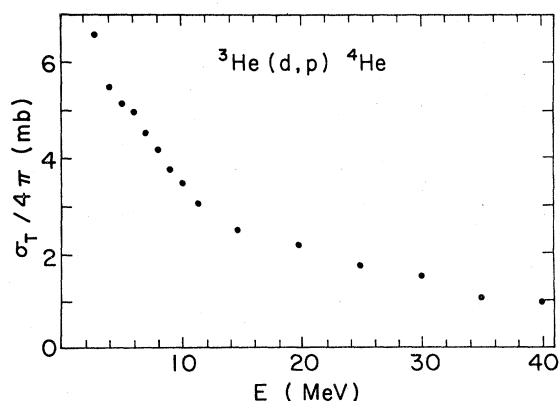


FIG. 11. Total cross section $\sigma_T/4\pi$ for the ${}^3\text{He}(d,p){}^4\text{He}$ reaction from the Legendre polynomial expansion analysis. The low energy results are taken from Ref. 41. The dots are larger than the uncertainties of the fits.

TABLE I. Total cross section values for the ${}^3\text{He}(d,d){}^3\text{He}$ reaction.

E_d (MeV)	$\sigma_{\text{TOT}}/4\pi$ (mb)
14.62	80.4 ± 0.4
19.69	75.0 ± 0.9
24.89	66.1 ± 1.3
30.02	61.2 ± 0.8
34.92	47.3 ± 0.4
39.95	37.6 ± 0.2

MeV points to a predominance of potential scattering and indicates only a weak dependence of the interaction on the spin of the target. Good optical model fits have been obtained between 10 and 14 MeV, using a very small tensor interaction, a spin-orbit term, and a surface absorption.⁴³ Consequently, the standard optical model potential was used here in the form

$$\begin{aligned}
 V_{\text{om}}(r) = & V_C(r_C) - V_f(r_v, a_v) - iWf(r_a, a_a) \\
 & + 4iW_D a_w \frac{d}{dr} f(r_w, a_w) \\
 & + \left[\frac{\hbar}{m_\pi c} \right]^2 (V_{\text{so}} + iW_{\text{so}}) \frac{1}{r} \frac{d}{dr} f(r_{\text{so}}, a_{\text{so}}) \vec{1} \cdot \vec{s},
 \end{aligned}$$

with

$$f(r_i, a_i) = \left[1 + \exp \frac{1}{a_i} (r - r_i A^{1/3}) \right]^{-1}.$$

The optical model fits were obtained by using the code MAGALI.⁴⁴

Starting values for the analyses were obtained by an inspection of previous analyses of deuteron scattering from light nuclei.^{43,45} During the initial runs it became apparent that both absorption terms W and W_{so} could indeed be set to zero without appreciably affecting the fits. Also, automatic searches were only successful if the surface diffuseness parameters a_w and a_{so} were kept constant until a fit was nearly obtained. Since average optimum values of $a_w = 0.35$ fm and $a_{\text{so}} = 0.30$ fm were found in grid searches throughout the energy range, they were always kept constant. This procedure resulted in the parameter set A of Table II. The resulting fits are given in Figs. 12 and 13 (solid lines). In order to get fits somewhat closer to the data at 35 and 40 MeV, it was necessary to

TABLE II. Potential parameters for d - ^3He elastic scattering.^a

	E_d	V	W_d	V_{so}	r_v	r_w	r_{so}	a_v	a_w	a_{so}
Set A										
	15	52.7	2.51	0.99	1.62	1.703	1.62	0.42	0.35	0.3
	20	55.1	3.36	2.75	1.62	1.703	1.62	0.42	0.35	0.3
	25	54.7	5.68	5.38	1.62	1.703	1.62	0.42	0.35	0.3
	30	57.0	5.94	5.16	1.62	1.703	1.62	0.42	0.35	0.3
	35	33.6	4.17	3.79	1.62	3.47	1.62	0.42	0.35	0.3
	40	33.1	3.77	4.70	1.62	3.38	1.62	0.42	0.35	0.3
Set B										
	15	160.9	2.82	2.14	1.6	2.6	2.0	0.317	0.317	0.317
	20	160.3	3.46	7.79	1.6	2.6	2.0	0.317	0.317	0.317
	25	159.6	4.11	8.15	1.6	2.6	2.0	0.317	0.317	0.317
	30	169.1	3.72	8.56	1.6	2.6	2.0	0.317	0.317	0.317
	35	160.1	6.03	10.70	1.7	3.0	1.7	0.25	0.317	0.25
	40	155.5	5.15	10.07	1.7	3.0	1.7	0.25	0.317	0.25
Set C										
	15	176.0	3.49	3.25	1.4	2.4	1.8	0.5	0.317	0.317
	20	200.6	4.17	4.97	1.3	2.4	1.8	0.5	0.317	0.317
	25	203.1	5.23	4.46	1.3	2.4	1.8	0.5	0.317	0.317
	30	215.4	6.28	2.67	1.3	2.2	1.8	0.4	0.317	0.317
Set D										
	15	171.9	3.53	4.56	1.417	2.688	1.868	0.5	0.317	0.317
	20	208.0	4.04	5.12	1.265	2.399	1.820	0.5	0.317	0.317
	25	206.6	5.20	4.77	1.284	2.393	1.765	0.5	0.317	0.317
	30	238.6	6.01	2.50	1.178	2.332	1.739	0.4	0.317	0.317

^aAll energies are given in MeV and lengths in fm.

use values for r_w quite different from the optimum average found for the lower energies. All other geometric parameters were kept the same at all energies; even so, the potential strengths W_d and V_{so} vary strongly with energy. A search on more free parameters would give a better fit at each energy but the parameters a and r would be fairly different from one set of data to another. For each set of parameters of Table II, the values were first varied to obtain the best fit for the 14.6 MeV data. Then those values became the starting values at the next higher energy. The procedure was subsequently repeated throughout the energy range.

Starting values based on averaged parameters from previous analysis on light nuclei⁵³ and more like the parameters obtained from another lower-energy analysis⁴⁰ made to represent the d - ^3He scattering in a study of the $^4\text{He}(p,d)^3\text{He}$ reaction led to set B of Table II. In this case it was attempted to keep all diffuseness values more or less

the same instead of the radius values (set A). Again, some parameters changed considerably above 30 MeV. However, the potential strengths changed in a less drastic way, when some geometric parameters were allowed to deviate strongly from their values at lower energy. Figures 12 and 13 show those fits as dashed lines. For the data up to 30 MeV, two other calculated curves are presented. The set C, generated from set B with smaller constant radii, leads to fits, in general, quite different from those originating from sets A and B. The set D, found by searching on radius values and potential strengths of set C, is not very different and the radii exhibit a variation with energy which is to be expected.

The three first sets of Table II represent distinct families based on different values of the product⁴⁶ $V(r_v)^n$ with $n \simeq 2$. The resulting fits display various features for each group of parameters, as can be seen in Figs. 12 and 13.

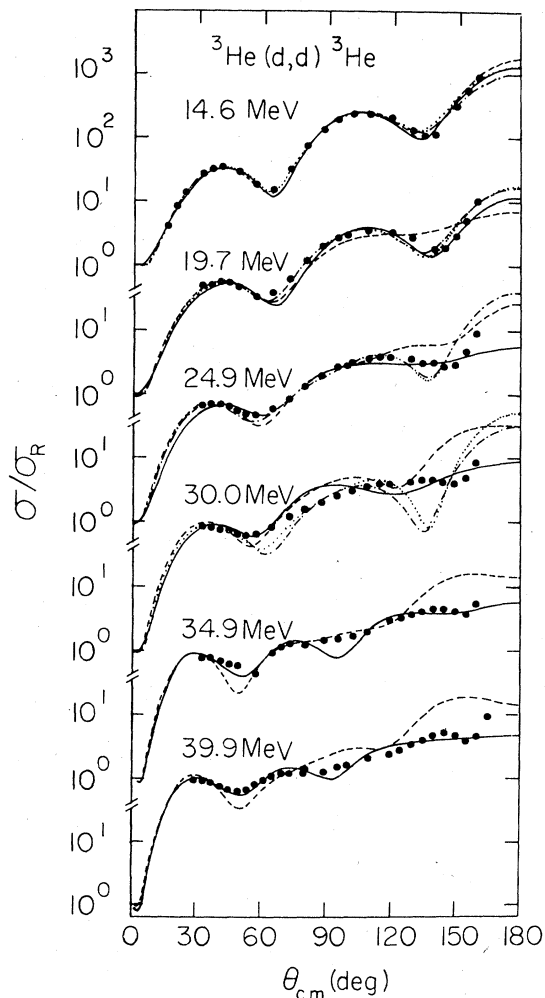


FIG. 12. Optical model fits of the cross section for the ${}^3\text{He}(d,d){}^3\text{He}$ scattering data between 14.6 and 40 MeV. The solid lines correspond to fits of set A (Table II), dashed lines to set B, dotted and dashed-dotted lines to sets C and D, respectively.

C. DWBA analysis of the ${}^3\text{He}(d,p){}^4\text{He}$ reaction

In the past, several analyses have been carried out on the ${}^3\text{He}(d,p){}^4\text{He}$ reaction. Diffraction and plane-wave Born approximation (PWBA) theories have been used at different energies^{37-39,47} around $E_p = 47$ MeV in the laboratory, but sophisticated PWBA theories were not appreciably more successful in representing the angular distributions.⁴⁷ The need of a lower cutoff in the radial overlap integrals to achieve reasonably good agreement was a common conclusion drawn from investigations with PWBA theory.^{38,47} A sensitivity to the lower cutoff radius was observed in the case of the

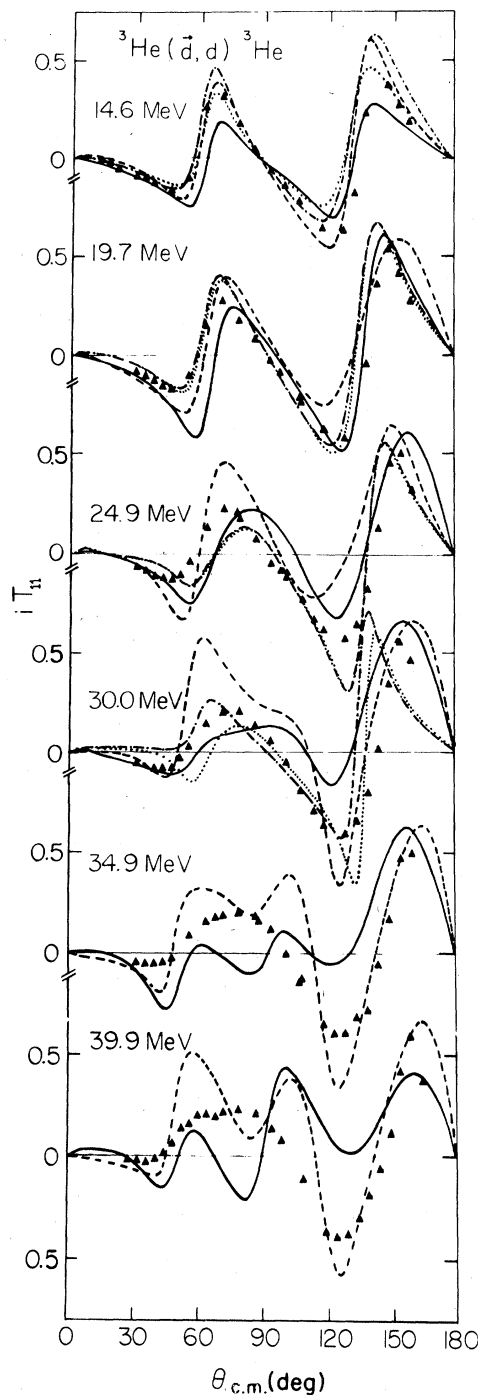


FIG. 13. Same as Fig. 12, but for the vector analyzing power data iT_{11} .

DWBA approach.³⁷⁻⁴⁷ A fairly good DWBA representation has been obtained³⁸ without a cutoff radius, but it was pointed out by the authors that the interpretation of the optical model parameters was ambiguous for both incident and exit channels.

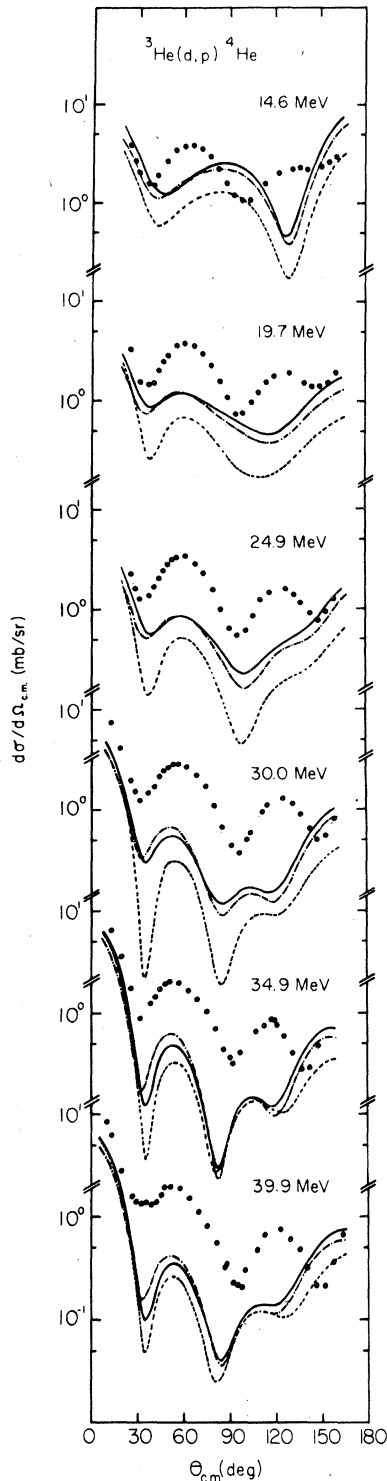


FIG. 14. DWBA calculations for the ${}^3\text{He}(d,p){}^4\text{He}$ cross sections with parameters of set *B* for the deuteron channel and from Ref. 48 for the proton channel. The solid lines were obtained in the zero range approximation, dashed-dotted lines, with a finite range correction of 1.25 fm, and dashed lines, with a cutoff radius of 3.0 fm.

In the present calculations, the code DWBA⁴⁸ has been used to obtain cross-section and vector analyzing-power angular distributions with the optical model parameters from Table II in the entrance channel and from an optical model analysis⁴⁹ of proton scattering on ${}^4\text{He}$ between 31 and 55 MeV. In the case of the proton channel, parameters corresponding to the closest c.m. energy have been chosen for each incident energy. Calculations in the zero range approximation (solid lines), with a finite range correction of 1.25 fm (dashed-dotted lines) and with a cutoff radius of 3 fm (dashed lines) are presented in Figs. 14 and 15. The computed curves are scaled as provided by the code, assuming a spectroscopic factor of 1.0. The different corrections applied do not change the general trend of the curves by much. The differential cross section tends, in general, to look more like the data at higher energy. Contrary to other calculations,⁴⁷ the d - ${}^3\text{He}$ optical model parameters currently used allow us to obtain computed curves with the general shape of the data, although a cutoff radius is not used. This is true for the cross section data above 20 MeV (Fig. 14). In fact, the data points do not show the deep minima characteristic of a cutoff radius.^{40,47} On the other hand, the corresponding analyzing power calculations (Fig. 15) show variations which are much too pronounced when compared to the data. The negative maximum at forward angles is well reproduced below 30 MeV, while the general shapes change around 30 MeV and a positive maximum at back angles is too large to reproduce the slight maximum found experimentally.

A finite range correction changes the computed curves very little, as shown in Figs. 14 and 15. Taking into account nonlocal effects does not affect the calculated angular distributions appreciably. However, changing the optical model parameters in the entrance channel does affect the shape of the curves quite seriously. As seen in Figs. 16 and 17, calculations at 15 and 30 MeV in the zero range approximation with set *A* in the entrance channel (dotted lines) look very different from results with set *B* (solid lines). Above 20 MeV, set *A* is not able to reproduce the back angle increase in the cross section. Nevertheless, set *C* calculations

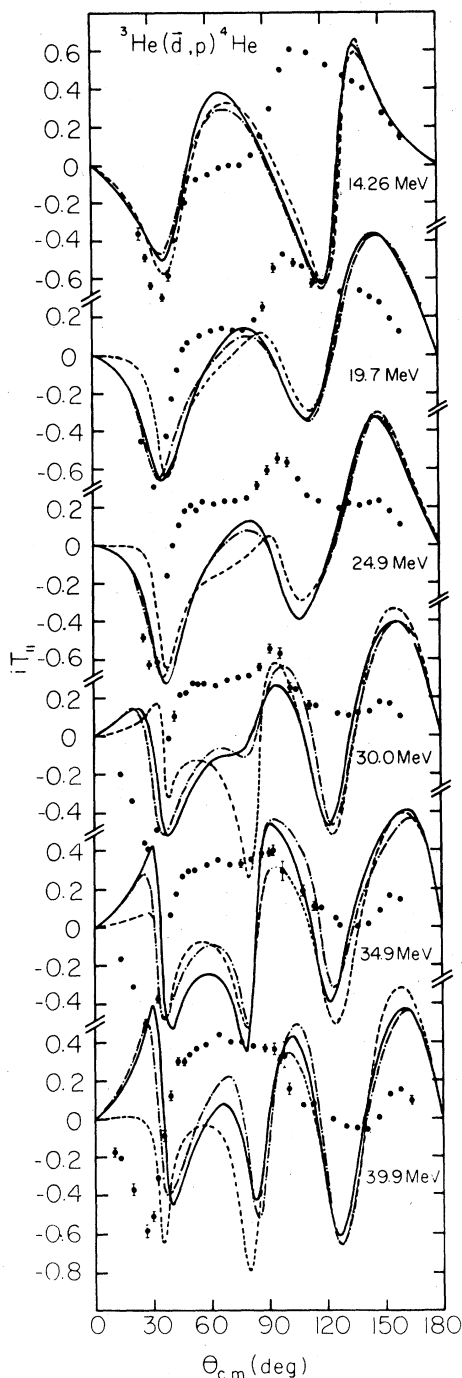


FIG. 15. Same as Fig. 14, but for the vector analyzing-power data iT_{11} .

(dashed-dotted lines), obtained in the zero range approximation, exhibit little change in the general shapes of the curves. The dashed lines at 30 MeV are zero range calculations provided by set *B* in the deuteron channel and by the p - ^4He parameters used

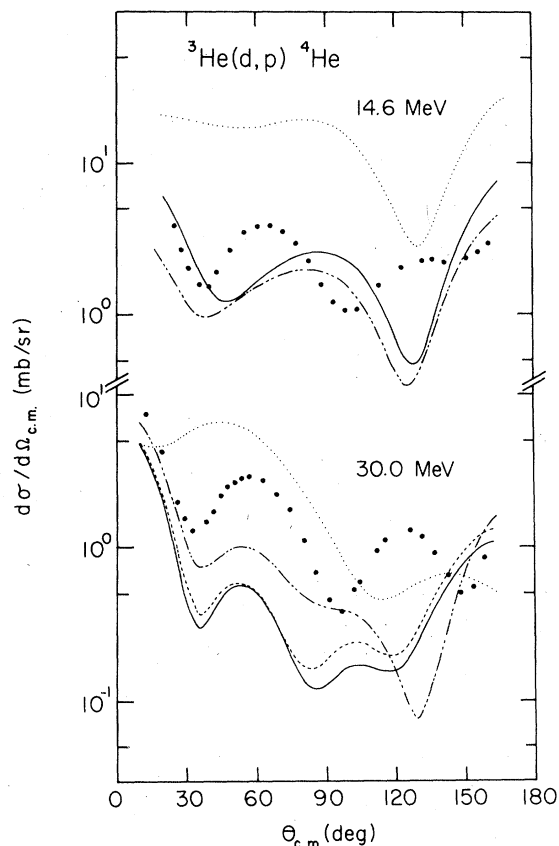


FIG. 16. DWBA calculations in zero range approximation with parameters of set *B* (solid lines), set *A* (dotted lines), and set *C* (dashed-dotted lines); the dashed line at 30 MeV is obtained with set *B* (d channel) and parameters (p channel) from Sawada *et al.* (Ref. 46).

by Sawada *et al.*⁴⁷; they show a limited influence of the parameters in the p channel. Finally, other calculations, not shown here, were made using the parameters from Thompson *et al.*⁴⁹ in the p - ^4He channel and different deuteron parameters. Whether made with finite range or nonlocality corrections or not, they gave results similar to those of Figs. 14 and 15 (set *B*) when the parameters of Sagle⁴⁰ in the d - ^3He channel are used and to those of Figs. 16 and 17 (dotted lines, set *A*) for the parameters of Lyorshin *et al.*⁴³ in the entrance channel. Thus, the deuteron parameters are again clearly separated into two categories; one family with $V \sim 50$ MeV and one with $V \sim 150$ – 200 MeV.

V. CONCLUSION

Some interesting features have been observed in the energy variations of the coefficients $d_{00}(L)$ and

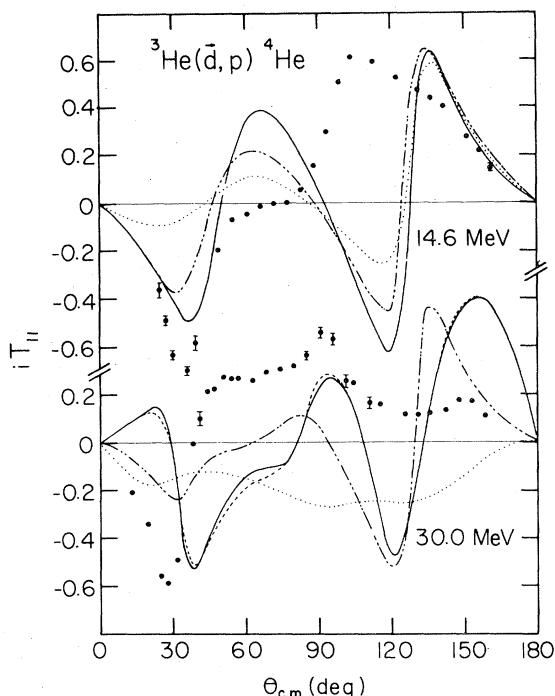


FIG. 17. Same as Fig. 16, for the vector analyzing-power data iT_{11} .

$d_{11}(L)$ obtained by a Legendre polynomial expansion of data on the ${}^3\text{He}(d,d){}^3\text{He}$ and ${}^3\text{He}(d,p){}^4\text{He}$ reactions. First, most of the coefficients show structures around 20 MeV and near 35 MeV deuteron energy with the exception of $d_{11}(L)$ of the ${}^3\text{He}(d,p){}^4\text{He}$ reaction. Second, the coefficient $d_{11}(2)$ of the ${}^3\text{He}(d,p){}^4\text{He}$ reaction is predominant at low energies, but with increasing energy the $L=1$ term becomes prevalent. This observation can be taken as a corroboration of the results of previous work,^{27,30,32} in which the presence of an f -wave $\frac{7}{2}^-$ state in the ${}^5\text{Li}$ system and the importance of the d -wave amplitudes was postulated.

Although the optical model analysis of the ${}^3\text{He}(d,d){}^3\text{He}$ elastic scattering between 15 and 40 MeV can give only a poor picture of the data at some energies, it seems to support the results of the Legendre polynomial analysis, since the optical model parameters (Table II) show a clear tendency for rapid change around 20–25 MeV and particularly at 35 MeV. However, an optical model analysis would be more conclusive if performed on a complete set of data using also a tensor polarized deuteron beam. It should be noted that such mea-

surements are also needed to reach more definite conclusions on the ${}^5\text{Li}$ system from an analysis of Legendre polynomial coefficients.

In general, the present fit to the angular distribution of the process ${}^3\text{He}(d,p){}^4\text{He}$ in the DWBA framework leads to the same conclusions as previous analyses. So, as pointed out in one of them,⁴⁷ the rise in the experimental differential cross section at back angles is reproduced by the calculated curves, even if only the single-particle pickup process is taken into account. The effect of introducing a cutoff radius is important and seems to be needed. The same holds, but to a lesser extent, with the optical model parameters provided by the d - ${}^3\text{He}$ elastic scattering analysis of Sec. IV B.

In fact, the usual way of accounting for nonlocal effects in DWBA calculations is not appropriate for reactions involving light nuclei.^{50,51} The contribution from the interior region must be dampened more strongly by the use of a cutoff radius. As suggested by Glendenning,⁵⁰ further investigations of such a reaction might provide a better agreement with the data, if they were based on the adiabatic model for the deuteron optical potential,⁵¹ a procedure already used in a few cases.^{51,52}

Finally, the calculations shown here allow discrimination between the different sets of optical model parameters for the d - ${}^3\text{He}$ channel. Set *A* of Table II, or parameters of the same family such as those from the work of Lyovshin *et al.*,⁴³ have to be excluded on the basis of the general shape of the differential cross sections (Fig. 16). In fact, this conclusion is only to be expected in view of the values of the parameters V , r_V , and r_W . Usually, the depth of the deuteron potential V is about twice that of the nucleon potential ($\sim 2 \times 50$ MeV) or more, while r_W is greater than r_V by about 40%.

ACKNOWLEDGMENTS

One of us (R.R.) is grateful for financial support through a fellowship from the Canadian Natural Sciences and Engineering Research Council and one of us (F.S.) is indebted to the Swiss National Science Foundation and the Max Geldner Stiftung for their assistance. This work was performed under the auspices of the U.S. Department of Energy.

- *Present address: Laboratoire de Physique Nucléaire, Université Laval, Québec, Canada, GIK 7P4.
- †Present address: Lovelace Foundation, ITRI, P.O. Box 5890, Albuquerque, New Mexico 87185.
- ‡Present address: Fermilab, Ms 306 P.O. Box 500, Batavia, Illinois 60510.
- ¹*Proceedings of the International Symposium on Polarization Phenomena in Nuclear Reactions, Zürich, (1975)*, edited by W. Grüebler and V. König, (Birkhäuser, Basel, 1976).
- ²*Proceedings on the 3rd International Symposium on Polarization Phenomena in Nuclear Reactions, Madison, 1970*, edited by H. H. Barschall and W. Haeberli (University of Wisconsin Press, Madison, 1971).
- ³F. Ajzenberg-Selove, Nucl. Phys. **A320**, 1 (1979).
- ⁴H. Grunder, R. Gleyvod, G. P. Lietz, G. Morgan, H. Rudin, F. Seiler, and A. Stricker, Helv. Phys. Acta. **44**, 622 (1971).
- ⁵J. W. Sunier, R. V. Poore, R. A. Hardekopf, L. Morrison, G. C. Salzmann, and G. G. Ohlsen, Phys. Rev. C **14**, 8 (1976).
- ⁶B. Jenny, W. Grüebler, V. König, P. A. Schmelzbach, R. Risler, D. O. Boersma, and W. G. Weitcamp, Ref. 1, p. 538.
- ⁷W. Grüebler, V. König, and P. A. Schmelzbach, Eidgenossische Technische Hochschule, Zürich, internal report, 1973.
- ⁸U. Rohrer, P. Huber, Ch. Leemann, H. Meiner, and F. Seiler, Helv. Phys. Acta. **44**, 899 (1971) and references therein.
- ⁹Ch. Leemann, H. Meiner, U. Rohrer, J. X. Saladin, F. Seiler, P. Huber, W. Grüebler, V. König, and P. Marmier, Ref. 2, p. 548.
- ¹⁰S. D. Baker, Ref. 2, p. 899.
- ¹¹Ch. Leemann, H. Bürgisser, P. Huber, H. Paetz gen. Schieck, and F. Seiler, Helv. Phys. Acta. **44**, 141 (1971).
- ¹²G. G. Ohlsen, R. A. Hardekopf, D. P. May, S. D. Baker, and W. T. Armstrong, Nucl. Phys. **A233**, 1 (1974).
- ¹³J. F. Clare, Nucl. Phys. **A217**, 342 (1973).
- ¹⁴J. E. Brock, A. Chisholm, J. C. Duder, R. Garrett, and R. E. White, Ref. 1, p. 546.
- ¹⁵G. S. Muetschler, W. B. Broste, and J. E. Simmons, Phys. Rev. C **3**, 1031 (1971).
- ¹⁶F. Seiler, E. Baumgartner, W. Haeberli, P. Huber, and H. R. Striebel, Helv. Phys. Acta. **35**, 385 (1962).
- ¹⁷W. B. Broste, G. P. Lawrence, J. L. McKibben, G. G. Ohlsen, and J. E. Simmons, Phys. Rev. Lett **25**, 1040 (1970).
- ¹⁸P. W. Lisowski, R. L. Walter, R. A. Hardekopf, and G. G. Ohlsen, Ref. 1, p. 887.
- ¹⁹R. A. Hardekopf, D. D. Armstrong, W. Grüebler, P. W. Keaton, Jr., and U. Meyer-Berkhout, Phys. Rev. C **8**, 1629 (1973).
- ²⁰R. A. Hardekopf, G. G. Ohlsen, R. V. Poore, and Nelson Jarmie, Phys. Rev. C **13**, 2127 (1976).
- ²¹G. G. Ohlsen, R. A. Hardekopf, R. L. Walter, and P. W. Lisowski, Ref. 1, p. 558.
- ²²N. T. Okumusoglu and C. O. Blyth, Nucl. Phys. **A235**, 45 (1979).
- ²³N. Simonious, in *Lecture Notes in Physics, Nuclear Physics*, edited by D. Fick (Springer, Berlin, 1974), Vol. 30, p. 38; Ref. 2, p. 401.
- ²⁴F. Seiler and E. Baumgartner, Nucl. Phys. **A153**, 193 (1970); Ref. 2, p. 518.
- ²⁵G. R. Plattner, A. D. Bacher, and H. E. Conzett, Phys. Rev. C **5**, 1158 (1972) and references therein.
- ²⁶N. E. Davison, S. A. Elbaker, A. Houdayer, A. M. Sourkes, W. T. H. van Oers, and A. D. Bacher, *Few Body Problem in Nuclear and Particle Physics*, edited by R. J. Slobodrian, B. Cujec, and K. Ramavataram (Les Presses de l'Université Laval, Québec, 1975), p. 539.
- ²⁷P. Heiss and H. H. Hackenbroich, Nucl. Phys. **A162**, 530 (1971).
- ²⁸H. H. Hackenbroich, Ref. 1, p. 133.
- ²⁹F. S. Chwieroth, R. E. Brown, Y. C. Tang, and D. R. Thompson, Phys. Rev. C **8**, 938 (1973).
- ³⁰F. Seiler, Nucl. Phys. **A187**, 379 (1972); **A244**, 236 (1975).
- ³¹D. C. Dodder and G. M. Hale (private communication).
- ³²K. Ramavataram and S. Ramavataram, Nucl. Phys. **A147**, 293 (1970).
- ³³H. E. Conzett, W. Dahme, Ch. Leemann, J. A. McDonald, and J. P. Meulders, Ref. 1, p. 566.
- ³⁴V. König, W. Grüebler, R. E. White, P. A. Schmelzbach, and P. Marmier, Nucl. Phys. **A185**, 263 (1972).
- ³⁵T. R. King and R. Smythe, Nucl. Phys. **A183**, 657 (1972).
- ³⁶R. W. Rutowski and E. E. Gross, Phys. Rev. C **12**, 362 (1975).
- ³⁷O. M. Bilaniuk and R. J. Slobodrian, Nucl. Phys. **50**, 585 (1964).
- ³⁸S. A. Harbison, R. J. Griffiths, N. M. Stewart, A. R. Johnston, and G. T. A. Squier, Nucl. Phys. **A152**, 503 (1970).
- ³⁹J. G. Rogers, J. M. Cameron, M. B. Epstein, G. Paic, P. Thomas, J. R. Richardson, J. W. Verba, and P. Doherty, Nucl. Phys. **A136**, 433 (1969).
- ⁴⁰A. Sagle, private communication and unpublished.
- ⁴¹W. Grüebler, V. König, A. Ruh, P. A. Schmelzbach, R. E. White, and P. Marmier, Nucl. Phys. **A176**, 631 (1970); W. Grüebler *et al.*, Ref. 7.
- ⁴²W. Klinger, F. Dusch, and R. Fleischmann, Nucl. Phys. **A166**, 253 (1971).
- ⁴³E. B. Lyovshin, O. F. Nemets, and A. M. Yasnogorodsky, Phys. Lett. **52B**, 392 (1974); Ref. 1, p. 542.
- ⁴⁴J. Raynal, Centre d'Etudes Nucléaires de Saclay Report No. DPh-T/69-42.
- ⁴⁵H. F. Bingham, A. R. Zander, K. W. Kemper, and N. R. Fletcher, Nucl. Phys. **A173**, 265 (1971); R. C. Brown, J. A. R. Griffith, O. Karban, L. Mesko, J. M. Nelson, and S. Roman, *ibid.* **A207**, 456 (1973); M. M.

- Meier and R. L. Walter, *ibid.* A182, 468 (1972).
- ⁴⁶See for instance, C. M. Perey and F. C. Perey, *Phys. Rev.* 132, 755 (1963).
- ⁴⁷T. Sawada, G. Paic, M. B. Epstein, and J. R. Rogers, *Nucl. Phys.* A141, 169 (1970).
- ⁴⁸J. M. Nelson and B. E. F. Macefield, Oxford University Nuclear Physics Laboratory Report 18/69, 1969 (unpublished).
- ⁴⁹G. E. Thompson, M. B. Epstein, and T. Sawada, *Nucl. Phys.* A142, 571 (1970).
- ⁵⁰N. K. Glendenning, in *Nuclear Spectroscopy and Reactions, Part D*, edited by J. Cerny (Academic, New York, 1975), p. 319; G. M. McAllen, W. T. Pinkston, and G. R. Satchler, *Part. Nucl.* 1, 412 (1971).
- ⁵¹R. C. Johnson and P. J. R. Soper, *Phys. Rev. C* 1, 976 (1970).
- ⁵²J. D. Harvey and R. C. Johnson, *Phys. Rev. C* 3, 636 (1971); G. R. Satchler, *ibid.* 4, 1485 (1971).
- ⁵³C. M. Perey and F. G. Perey, *At. Data Nucl. Data Tables* 17, 1 (1976).